Published in final edited form as:
Am J Physiol Heart Circ Physiol. 2014 February 15; 306(4): H564–H573. doi:10.1152/ajpheart.00441.2013.

Enhanced currents through L-type calcium channels in cardiomyocytes disturb the electrophysiology of the dystrophic heart

Xaver Koenig[#1], **Lena Rubi**[#1], **Gerald J. Obermair**[3], **Rene Cervenka**[1], **Xuan B. Dang**[1], **Peter Lukacs**[1], **Stefan Kummer**[2], **Reginald E. Bittner**[2], **Helmut Kubista**[1], **Hannes Todt**[1], and **Karlheinz Hilber**[1,*]

[1]Center for Physiology and Pharmacology, Medical University of Vienna, Vienna, Austria

[2]Center for Anatomy and Cell Biology, Medical University of Vienna, Vienna, Austria

[3]Department of Physiology and Medical Physics, Medical University Innsbruck, Innsbruck, Austria

[#] These authors contributed equally to this work.

Abstract

Duchenne muscular dystrophy (DMD), induced by mutations in the gene encoding for the cytoskeletal protein dystrophin, is an inherited disease characterized by progressive muscle weakness. Besides the relatively well characterized skeletal muscle degenerative processes, DMD is also associated with cardiac complications. These include cardiomyopathy development and cardiac arrhythmias. The current understanding of the pathomechanisms in the heart is very limited, but recent research indicates that dysfunctional ion channels in dystrophic cardiomyocytes play a role. The aim of the present study was to characterize abnormalities in L-type calcium channel function in adult dystrophic ventricular cardiomyocytes. By using the whole cell patch clamp technique, the properties of currents through calcium channels in ventricular cardiomyocytes isolated from the hearts of normal and dystrophic adult mice were compared. Besides the commonly used dystrophin-deficient mdx mouse model for human DMD, we also used mdx-utr mice which are both dystrophin- and utrophin-deficient. We found that calcium channel currents were significantly increased, and channel inactivation was reduced in dystrophic cardiomyocytes. Both effects enhance the calcium influx during an action potential (AP). Whereas the AP in dystrophic mouse cardiomyocytes was nearly normal, implementation of the enhanced dystrophic calcium conductance in a computer model of a human ventricular cardiomyocyte considerably prolonged the AP. Finally, the described dystrophic calcium channel abnormalities

[*]**Corresponding Author:** Karlheinz Hilber, Center for Physiology and Pharmacology, Department of Neurophysiology and -pharmacology, Medical University of Vienna, Schwarzspanierstrasse 17, 1090 Vienna, Austria. Telephone: ++43 1 40160 31230; Fax: ++43 1 40160 931300; karlheinz.hilber@meduniwien.ac.at.

Disclosures

No conflicts of interest, financial or otherwise, are declared by the authors.

Author Contributions

The experiments of this study were performed at the Center for Physiology and Pharmacology (Medical University of Vienna), and the Department of Physiology and Medical Physics (Medical University of Innsbruck). Specific contributions are as follows: conception and design of experiments: X.K., L.R., G.J.O., H.T., and K.H.; collection, analysis and interpretation of data: X.K., L.R., G.J.O, R.C., X.B.D., P.L., S.K., R.E.B., H.K., H.T., and K.H.; drafting the article or revising it critically for important intellectual content: X.K., L.R., G.J.O, R.C., X.B.D., P.L., S.K., R.E.B., H.K., H.T., and K.H. All authors approved the final version of the manuscript.

Europe PMC Funders Author Manuscripts

entailed alterations in the electrocardiograms of dystrophic mice. We conclude that gain of function in cardiac L-type calcium channels may disturb the electrophysiology of the dystrophic heart and thereby cause arrhythmias.

Keywords

cardiac action potential; Duchenne muscular dystrophy; L-type calcium channels; dystrophin-deficient mouse models; ventricular cardiomyocytes

Introduction

Duchenne muscular dystrophy (DMD) is an inherited disease characterized by progressive muscle weakness and degeneration. It is the most common and devastating form among the human muscular dystrophies, and affected patients suffer from loss of ambulation, respiratory failure, and premature death. The gene defect for DMD was mapped to an X chromosome gene encoding for the intracellular protein dystrophin. Dystrophin interacts with proteins of the so-called dystrophin-associated protein complex (DAPC) (11), and serves as a linker between the cytoskeleton and the extracellular matrix. Progressive skeletal muscle wasting in DMD is also accompanied by severe cardiac complications. These include cardiomyopathy development and arrhythmias (33) and significantly contribute to the morbidity and mortality observed (6). The mechanisms causing these cardiac complications, however, are largely unclear.

Dystrophin and other protein members of the DAPC interact with voltage-gated ion channels. For example, the C termini of muscle and brain sodium channels bind to the PDZ domain of multiple members of the syntrophin family of dystrophin-associated proteins (13). Disruption of such DAPC interactions with ion channels impairs their functional properties. Thus, dystrophin-deficiency in cardiomyocytes from the mdx mouse (most commonly used mouse model for human DMD with a mutation in the dystrophin gene) induces reduced sodium current densities and altered gating properties in cardiac $Na_v1.5$ sodium channels (2; 12). Importantly, decreased sodium currents in cardiomyocytes can explain impairments in cardiac impulse conduction observed in DMD patients (e.g. (27)). This exemplarily points out how the disruption of a DAPC interaction with a voltage-gated ion channel may induce cardiac complications associated with DMD.

Besides sodium channels, voltage-gated calcium channels also play an essential role in cardiomyocytes. In particular, cardiac L-type $Ca_v1.2$ channel activity determines the plateau phase of the cardiac action potential (AP) and initiates contraction. Mutations in genes encoding for $Ca_v1.2$ cause various disease phenotypes including Timothy syndrome, Brugada syndrome, and early repolarization syndrome (35). This highlights the importance of a proper function of this channel in the heart. Little is known about L-type calcium channel abnormalities in the dystrophic heart. Isolated cardiomyocytes from mdx mice show elevated intracellular calcium levels (38). It is, however, unclear if abnormal L-type calcium channel activity contributes to this phenomenon (39), because here other mechanisms such as stretch-dependent ones may play a more prominent role (8; 38). In mouse cardiomyocytes $Ca_v1.2$ colocalizes with dystrophin, and cardiomyocytes derived from dystrophin-deficient

Europe PMC Funders Author Manuscripts

mdx mice show impaired calcium channel inactivation (29). We could recently confirm the reduced calcium channel inactivation in dystrophic cardiomyocytes (20). Both (29) and our study (20) were performed on cardiomyocytes derived from neonatal dystrophic mice. Although a frequently used model cell system, the electrophysiological properties of neonatal cardiomyocytes do not well reflect the situation in the adult heart (e.g. (19; 20)). Therefore, it is currently unclear if, and to what extent, calcium channel abnormalities do also exist in the adult dystrophic heart.

The aim of the current work was to characterize abnormalities in L-type calcium channel function in adult dystrophic ventricular cardiomyocytes. Besides using the classical dystrophin-deficient mdx mouse, here, for the first time, we also used mice additionally carrying a mutation in the utrophin gene (9; 14). The latter mouse model (mdx-utr) more closely resembles the general pathology observed in DMD patients, and develops a more severe cardiomyopathy with an earlier onset compared to mdx (14; 16). Comparison of mdx with mdx-utr enabled us to test whether the stronger cardiac phenotype of the double-mutant mice correlates with more severe calcium channel abnormalities, as we (20) and (2) recently reported for malfunctions in the cardiac sodium channel $Na_v1.5$. Finally, we tested the consequences of the observed calcium channel abnormalities in dystrophic cardiomyocytes on the cardiac action potential (AP), as well as on the electrocardiograms of neonatal and adult dystrophic mice.

Materials and Methods

Ethical approval

The investigation conforms to the guiding principals of the Declaration of Helsinki and coincides with the rules of the University Animal Welfare Committee. For animal research, approval was granted by the Austrian Ministry for Science and Research (BMWF-66.009/0211-II/10b/2009).

Mouse models

Wild type (wt) C57BL/6 mice, dystrophin-deficient mdx (31), and dystrophin/utrophin-deficient double mutant mdx-utr (9; 14) mice, backcrossed on the C57BL/6 background for more than 12 generations, were used for the work. The mdx mouse lacks full length dystrophin due to a mutation that results in a premature stop codon in exon 23. In the utr mouse, a neomycin cassette was introduced into exon 7 of the utrophin gene to disrupt the reading frame. For the calcium current measurements, and for action potential recordings at 7 Hz pacing frequency, mdx mice on the BL10 background (C57BL/10ScSn-*Dmd*^{mdx}/J) and respective wt control mice (C57BL/10ScSnJ) were recently purchased from Charles River Laboratories. Throughout the text, the c‘‘mdx’’. Double mutant (dystrophin-/- and utrophin-/-) mice are termed ‘‘mdx-utr’’. Genotyping of the mice was performed by using standard PCR-assays. For any comparisons between mdx and mdx-utr, littermates were used in the electrophysiological experiments.

Isolation of adult ventricular cardiomyocytes

4-6 months old female mice were killed by cervical dislocation, and ventricular cardiomyocytes were isolated from their hearts as in our previous study (20). Only female animals were used here in order to exclude possible artefacts introduced by gender differences, and to allow for direct comparability with the results obtained in (20).

Barium current recordings

Currents were recorded in the whole cell patch clamp mode from adult cardiomyocytes up to 8 hours after preparation at a temperature of 22 ± 1.5°C, using an Axoclamp 200B patch clamp amplifier (Axon Instruments, Union City, CA). Pipettes were formed from aluminosilicate glass (AF150-100-10; Science Products, Hofheim, Germany) with a P-97 horizontal puller (Sutter Instruments, Novato, CA), and had resistances between 0.8 and 1.5 MΩ when filled with the respective pipette solution (see below). Data acquisition was performed with the pClamp 6.0 software (Axon Instruments) through a 12-bit A-D/D-A interface (Digidata 1200; Axon Instruments). Data were low-pass filtered with 2 kHz (-3 dB) and digitized at 5 kHz. Capacity transients and leak currents were subtracted using a P/4 protocol. Data analysis was carried out using Clampfit 10.2 (Axon Instruments) and GraphPad Prism 5.01 (San Diego, USA) software. The external solution contained 10 mM BaCl2, 145 mM TEA-Cl, 10 mM Hepes, pH = 7.4 adjusted with TEA-OH. The internal solution contained 145 mM Cs-aspartate, 2 mM $MgCl_2$, 10 mM Hepes, 0.1 mM Cs-EGTA, 2 mM Mg-ATP, pH= 7.4 adjusted with CsOH. The kinetics of barium current inactivation (representing voltage-dependent calcium channel inactivation) was analysed as follows: the current decay after channel activation was fit with a single exponential function to derive time constants (τ-values). Current-voltage relationships were fit with the function: $I(V)=G_{max}*(V-V_{rev})/(1+\exp((V_{0.5}-V)/K))$ where I is the current, G_{max} is the maximum conductance, V is the membrane potential, V_{rev} is the reversal potential, $V_{0.5}$ is the voltage at which half-maximum activation occurred, and K is the slope factor. Steady-state fast inactivation data were fit with the Boltzmann function: $I/Imax = 1/(1+\exp((V-V_{0.5})/K))$ where I/Imax is the normalized current, and the other parameters are defined as above. Recovery from inactivation was tested by applying a 5 s inactivating pre-pulse to 20 mV, which was followed by a 100 ms test pulse to 20 mV after various time intervals (in ms: 0.1, 1, 10, 30, 100, 300, 1000, 10000, 30000). Gating currents were elicited from a holding potential of -80 mV by a depolarizing step to -20 mV. This particular potential was chosen because it moved a considerable amount of gating charge without triggering barium influx (see Fig. 1F). A similar approach was used in (37). Smaller depolarizations (e.g. to -40 mV) did not elicit any detectable gating currents, whereas larger depolarizations (e.g. to 0 mV) triggered a barium inward current on top of the gating current. On-gating charge (Q_{on}) was determined by integrating the gating current over time and normalized to the cell capacitance.

Calcium current recordings

Whole cell calcium currents were recorded from adult cardiomyocytes derived from wt and mdx mice. The kinetics of calcium current inactivation (representing both calcium- and voltage-dependent calcium channel inactivation) was analyzed by measuring the time period

between the current peak, and the time point at which the current had decayed to 50%. This parameter, which was also used in our previous study (20), is termed “decay half-time”. The solutions used to record calcium currents were identical to those used for the barium current recordings, except that the external solution contained 10 mM $CaCl_2$ instead of 10 mM $BaCl_2$.

Potassium current recordings

Whole cell potassium currents were recorded in an external solution containing 140 mM NaCl, 4 mM KCl, 2 mM $CaCl_2$, 2 mM $MgCl_2$, 5 mM Hepes, 5 mM Glucose, pH= 7.4 adjusted with NaOH. The pipette solution consisted of 10 mM NaCl, 140 mM KCl, 2 mM EGTA, 1 mM $MgCl_2$, 0.1 mM Na-GTP, 5 mM Mg-ATP, 10 mM Hepes, pH= 7.2 adjusted with KOH.

Action potential recordings

APs were recorded from adult cardiomyocytes in the current-clamp mode of the whole cell patch clamp technique. APs were elicited both at 1 and 7 Hz by rectangular current pulses of a duration of 4 ms at 125% threshold level. Data were low-pass filtered with 10 kHz (-3 dB) and digitized at 100 kHz. The bath and pipette solutions were identical to the solutions used for the potassium current measurements.

Computer simulations of mouse and human ventricular action potentials

Computer models for mouse ((4), apical version) and human ((34), mid-myocardial version) ventricular cardiomyocytes were downloaded from http://www.cellml.org/models. All simulations were performed in the CellML environment (22) with the default parameters of the models. Action potentials were simulated with a step size of 0.01 and 0.1 ms for mouse and human simulations, respectively. The impact of the L-type calcium channel in these models was studied by systematic variation of its conductance g_{CaL} from 0.25 – 4-fold of its default value. The experimentally observed increase in L-type calcium channel conductance in adult dystrophic cardiomyocytes was implemented by increasing the default value 1.6-fold. The experimentally determined “dystrophic” deceleration in barium current decay was simulated by adjusting the inactivation time constant τ_f of the model to “mod. τ_f“. This was done as follows: In the tenTuscher model of a ventricular cardiomyocyte (34), ICaL is implemented as a Hodgkin-Huxley type formalism. To include the observed changes in current decay (Fig. 1C) into our simulations we had to amend the voltage-dependent inactivation gate f of ICaL of the tenTuscher model. The voltage-dependence of steady-state inactivation, f_∞, was left unchanged in accordance with our experimental data. The time constant of inactivation, τ_f, was first adjusted to fit our experimental wt data, from default

$$\tau_f = 1125.e^{-(V+27)^2/240} + \frac{165}{1+e^{(25-V)/10}} + 80$$

to

$$\tau_f = 140.e^{-(V+27)^2/700} + \frac{165}{1+e^{(25-V)/10}} + 75.$$

This adjustment did not lead to visible alterations in the simulated APs. To include the deceleration in current decay as observed in the dystrophic cardiomyocytes (Fig. 1C), τ_f was then changed to:

$$mod.\tau_f = 450.e^{-(V+27)^2/700} + \frac{165}{1+e^{(25-V)/10}} + 75.$$

RNA isolation and quantitative Taqman-PCR

Taqman RT-PCR on RNA isolated from heart tissue was performed according to a previously developed protocol (30). For isolation of RNA, hearts of 10–16 week old animals were shock frozen in isopentane cooled on dry ice. For each specimen, 20 mg of ventricular tissue (from apex, approx. 200 slices with a slice thickness of 5 μm) was cut with a microtome at −20°C. Frozen tissue slices were immediately resuspended in RTL lysis buffer of the RNeasy Fibrous Tissue Kit (Qiagen, Vienna, Austria). RNA was isolated according to the manufacturer's protocol. RNA concentrations were determined photometrically using a Nanodrop spectrophotometer (Thermo Fisher Scientific, Waltham, MA, USA). Reverse transcription was performed on 1 μg of RNA using Superscript II reverse transcriptase (Invitrogen, Carlsbad, USA) and random hexamer primers (Promega, Madison, USA); RT mix was incubated for 60 min at 37°C. The relative abundance of different CaV subunit transcripts was assessed by TaqMan quantitative PCR (qRT-PCR) using a standard curve method based on PCR products of known concentration in combination with normalization using the most stable control genes as previously described (30). TaqMan gene expression assays specific for $Ca_v1.2$, $Ca_v1.3$, $\alpha_2\delta$-1, and β_2, designed to span exon–exon boundaries, were purchased from Applied Biosystems (Foster City, CA). The following assays were used [name (gene symbol), assay ID (Applied Biosystems)]: $Ca_v1.2$ (Cacna1c), Mm00437953 m1; $Ca_v1.3$ (Cacna1d), Mm01209919 m1; β_2 (Cacnb2), Mm00659092 m1; $\alpha_2\delta$-1 (Cacna2d1), Mm00486607 m1. The endogenous control genes included were [name (gene symbol), assay ID (Applied Biosystems)]: b-cytoplasmic actin (Actb), Mm00607939 s1; beta-2-microglobulin (B2m), Mm00437762 m1; glyceraldehyde-3-phosphate dehydrogenase (Gapdh), Mm99999915 g1; hypoxanthine phosphoribosyl-transferase 1 (Hprt1), Mm00446968 m1; succinate dehydrogenase complex, subunit A (Sdha), Mm01352363 m1; tata box binding protein (Tbp), Mm00446973 m1; transferrin receptor (Tfrc), Mm00441941 m1. qRT-PCR (50 cycles) was performed in duplicates using 20 ng total RNA equivalents of cDNA and the specific TaqMan gene expression assay for each 20 μl reaction in TaqMan Universal PCR Master Mix (Applied Biosystems). Measurements were performed on three independent RNA preparations from each genotype. Analyses were performed using the 7500 Fast System (Applied Biosystems). The Ct values for each C_{av} gene expression assay were recorded for each individual preparation. To allow a direct comparison between the expression levels in different samples, we normalized all experiments to Hprt1 and Gapdh, which were determined to be most stably expressed

Europe PMC Funders Author Manuscripts

reference genes across all preparations and time points. Subsequently, normalized molecule numbers were calculated for each C_{av} subunit from their respective standard curve (30). Data were organized and analyzed using MS Excel and SPSS statistical software (SPSS Inc, Chicago IL, USA). Statistical significance was determined by two-way ANOVA.

Surface electrocardiogram recordings

Standard 6-lead surface electrocardiograms (ECGs) were recorded from conscious neonatal mice 2 and 12 (9-14 day-old; mean, 12.3) days of age. ECGs were also recorded from anaesthetized adult female mice in two different time windows (4-6 months; mean, 140 days and 8-21 months; mean, 420 days). A mean animal age of 140 days resembles the age of the mice (4-6 months) used for cardiomyocyte isolation. Because of the reduced lifespan of mdx-utr mice, ECG recordings on 420 day-old animals could only be performed on wt and mdx mice. ECG recordings from neonatal mice were performed as in our previous study (20). A custom-built setup restrained neonatal mice in movement. Four Ag/AgCl-electrode footpads were used to record ECGs. The pads were wetted with ECG electrode gel, and each foot was placed such that it made contact with a separate electrode. Adult mice were anaesthetized with a single ip injection of 350 mg/kg chloral hydrate, and depth of anesthesia was monitored (minimal response to hind-foot pinch). Small-needle ECG leads were placed subcutaneously on all 4 extremities. Body temperature was maintained at 37°C using a heating pad and lamp. Signals were amplified (Gould model 11 G412301; Gould Inc., Cleveland, Ohio, USA), high- and low-pass filtered with -3 dB cut-off frequencies of 0.3 and 1 kHz, respectively, digitized at 5 kHz, and stored for offline analysis. To reduce noise levels, ECG signals were averaged over 50-200 beats prior to evaluation. Interval values were normally determined by calculating the mean of all 6 standard leads. Individual values which could not be unambiguously identified were excluded from the succeeding analysis. The RR interval was determined as average distance between 50-200 consecutive QRS complexes (Fig. 5A). Heart rate in beats per minute (bpm) was then calculated as: 60000/RR (ms). The PQ interval was measured from the beginning of the P wave to the beginning of the QRS complex (Fig. 5A). The QT interval was measured from the end of the PQ interval to the time point at which the ECG signal approached the isoelectric line just before the rise of the next P wave (Fig. 5A, inset). The heart rate-dependence of the QT interval was corrected assuming a linear relation between the QT interval and the RR interval. Experimental data from all three genotypes were fit with a linear regression model with the formula: $QT=k*RR+c$, where k and c are the regression parameters which represent the steepness and the QT offset value at an RR interval of 0 ms, respectively. Corrected QT interval values (QTc) were calculated referring to an RR interval of 100 ms (heart rate of 600 bpm). Wherever in the text we present or interpret our QT interval data, we refer to QTc values.

Statistics

Data are expressed as means ± SEM if not otherwise specified. Except for the RT-PCR experiments (see above), statistical comparisons between wt, mdx, and mdx-utr were made using one-way ANOVA (for independent samples) with Tukey's Post Hoc test. In case only two groups had to be compared, an unpaired two-tailed Student's t-test was performed. A p-value <0.05 was considered significant.

Results

L-type calcium channel properties in normal and dystrophic cardiomyocytes. Figure 1A shows typical original traces of barium currents, elicited by the pulse protocol displayed on top, of a wild type (wt), mdx, and mdx-utr cardiomyocyte. A summary of the current density-voltage relationships, derived from a series of such experiments, is presented in B. It can be observed that the current densities of dystrophic cardiomyocytes were significantly increased compared to those in wt cells. The current densities of mdx and mdx-utr cardiomyocytes, on the other hand, were similar. This suggests that dystrophin-deficiency (mdx and mdx-utr) alone, but not extra utrophin-deficiency (only mdx-utr) generated the observed increase in current density.

Analysis of the current decay after channel activation (Fig. 1C) revealed that the kinetics of voltage-dependent inactivation was considerably slowed in dystrophic cardiomyocytes. Significant differences at certain voltages were assessed by single exponential decay current fits (Fig. 1C). Again mdx and mdx-utr cardiomyocytes were similar. These data suggest that, in addition to an increase in current density, dystrophin-deficiency also generated a reduction in voltage-dependent calcium channel inactivation. To test if besides voltage-dependent inactivation also calcium-dependent inactivation is impaired in dystrophic cardiomyocytes, additional experiments were performed using calcium instead of barium as the charge carrier. Fig. 1D shows that the kinetics of calcium current inactivation was significantly slowed in mdx compared to wt cardiomyocytes. This suggests that dystrophin-deficiency also caused a reduction in calcium-dependent channel inactivation. Figure 1E finally shows that both steady-state inactivation (left) and the recovery from inactivation (right) were similar in wt and dystrophic cardiomyocytes.

In order to study if a greater number of functional calcium channels in the membrane may account for the observed current density increase in dystrophic compared to wt cardiomyocytes (Fig. 1B), we evaluated ON-gating charge (Q_{on}) values from gating currents elicited by depolarizing voltage steps to -20 mV (see Methods and Fig. 1F, left). These Q_{on} values, which represent a simple measure of the number of channels in the membrane, were similar in wt and dystrophic cells. As a result, a linear regression of the current density with Q_{on} forced through the origin (Fig. 1F, right) revealed steeper slopes for mdx (k=3.4, dashed line) and mdx-utr (k=3.2, dotted line) compared to wt (k=1.6, solid line). For all genotypes, a significant linear relationship ($p<0.01$, F-test) existed between Q_{on} and current density. These data suggest that altered single channel properties, but not a higher number of functional calcium channels in the membrane, are responsible for the increased current densities observed in dystrophic cardiomyocytes.

To test the hypothesis that an altered L-type calcium channel subunit expression in dystrophic cardiomyocytes may be responsible for the abnormal channel properties in these cells, we performed quantitative RT-PCR experiments on ventricular tissue derived from wt, mdx, and mdx-utr hearts. Fig. 2 shows that the mRNA levels of all the studied calcium channel subunits were similar in the hearts of wt and dystrophic animals. This was true for the main cardiac α_1 channel subunit α_{1C} ($Ca_v1.2$), as well as for its auxiliary subunits $\alpha_2\delta$-1 and β_2. Finally, α_{1D} ($Ca_v1.3$), which is normally insignificantly expressed in the adult

cardiac ventricle (7), did not seem to be abnormally induced in the dystrophic heart. Under the assumption that the amount of translated protein parallels the transcription of mRNA, these data not only confirmed that the number of calcium channels was similar in wt and dystrophic cardiomyocytes (see above); they also suggest that auxiliary calcium channel subunit expression was normal in the dystrophic heart.

Action potentials in normal and dystrophic cardiomyocytes

To estimate the effects of the abnormal L-type calcium channel properties in dystrophic cardiomyocytes on the cardiac AP, we recorded APs at different pacing frequencies from wt, mdx and mdx-utr cardiomyocytes, typical examples of which are displayed in Fig. 3A (1Hz) and C (7 Hz). In Fig. 3B (1 Hz) and D (7 Hz), AP durations at 25% and 75% repolarization (left), and AP areas (right) were compared between wt and dystrophic cardiomyocytes. It can be observed that, at both pacing frequencies, no significant differences between wt and dystrophic cells were present among the tested groups in any of these parameters. This suggests that AP duration was similar in wt and dystrophic cardiomyocytes.

Because it was surprising that the observed abnormalities in L-type calcium channel properties in dystrophic cardiomyocytes (e.g. a profound increase in current density) did not significantly prolong the AP in these cells, we sought for an additional confirmation of this finding. A computer model of a mouse ventricular cardiomyocyte (4) in which we implemented the enhanced calcium conductanceof dystrophic cardiomyocytes (1.6-fold g_{CaL} compared with wt) indeed confirmed the results of our experiments (Fig. 3E). Namely, we found no considerable AP prolongation under the simulated condition of an increased “dystrophic” calcium conductance. In addition, systematic variation of g_{CaL} over a wide range (0.25- to 4-fold) in these simulations suggested that the impact of calcium conductance on the shape of the mouse AP is small in general. Thus, only 4-fold g_{CaL} caused a readily discernible change in AP form (Fig. 3E).

Finally, considering the substantial differences between the cardiac AP in mouse and men (25), it was of interest to additionally use a computer model of a human ventricular cardiomyocyte (34) (Fig. 3F), and to execute the same simulations as described above. Interestingly, under increased “dystrophic” calcium conductance (1.6-fold g_{CaL} compared with wt), in contrast to the mouse AP, the human AP was considerably prolonged. Further, variation of g_{CaL} over a wide range also revealed a much bigger effect of calcium conductance in shaping the human (Fig. 3F, left) compared with the mouse (Fig. 3E) AP. Besides the increased dystrophic calcium conductance, implementation of the experimentally observed deceleration in voltage-dependent inactivation in dystrophic cardiomyocytes into the human AP simulations yielded an additional AP-prolonging effect (Fig. 3F, right).

Potassium currents in normal and dystrophic cardiomyocytes

An alternative explanation for the lack of an AP-prolonging effect of the observed L-type calcium channel abnormalities in mdx and mdx-utr cardiomyocytes would be enhanced potassium outward currents in dystrophic cells, which counteract the impact of increased calcium inward currents. To test this hypothesis we compared outward potassium currents in

wt, mdx, and mdx-utr cardiomyocytes. Fig. 4 shows that no significant differences existed between the potassium current densities in wt and dystrophic cardiomyocytes, whereby a tendency towards decreased currents in dystrophic cells can be observed. These experiments suggest that the potassium outward currents in dystrophic cardiomyocytes are not enhanced, and therefore cannot counteract the effects of increased calcium currents in these cells.

Surface electrocardiogram (ECG) recordings on normal and dystrophic mice

To test if abnormal calcium channel function at the cellular level in dystrophic cardiomyocytes affects the heart's electrophysiological properties in dystrophic animals, we compared ECGs of wt and dystrophic mice. In order to be able to track developmental changes, here, animals over a broad age range (2 to 420 days, see Methods) were studied. This also allowed for comparison with our earlier work (20) in which we reported L-type calcium channel abnormalities in dystrophic cardiomyocytes derived from neonatal mice. Figure 5A shows typical examples of ECG recordings on a neonatal wt (top left) and an adult wt (top right) mouse, and the corresponding traces obtained by averaging of 100 original traces (lower panel). We found that, at all animal ages tested, the heart rate was similar in wt and dystrophic animals (Fig. 5B). On the other hand, the PQ intervals of the ECGs were significantly shortened in dystrophic mice over the whole age range (Fig. 5C). No significant differences existed between the PQ intervals of mdx and mdx-utr mice in the respective age groups. Finally, the QT intervals of the ECGs were similar in neonatal wt and dystrophic animals (Fig. 5D, left). In adult dystrophic mice, the QT intervals tended to be slightly prolonged (Fig. 5D, right), whereby a significant difference was present only in the oldest age group (420 days, wt versus mdx). Again no difference existed between the QT intervals of mdx and mdx-utr mice over the whole animal age range tested.

Discussion

Calcium channel abnormalities in adult dystrophic cardiomyocytes

Here we report significant L-type calcium channel abnormalities in ventricular cardiomyocytes derived from adult dystrophic mice: first, current density is 1.6-fold increased, and secondly, calcium channel inactivation is considerably reduced in dystrophic cardiomyocytes. Importantly, both effects will enhance the calcium influx during an AP. Calcium channel inactivation occurs by two mechanisms: a slow, voltage-dependent mechanism, and a faster, calcium-dependent mechanism (15). In the present study, by performing two sets of current recordings with either barium or calcium as the charge carrier, we could provide evidence that both voltage-dependent and calcium-dependent channel inactivation are impaired in dystrophic cardiomyocytes. A recent study, which was published in the course of writing up of this manuscript (36), confirmed a significantly slowed calcium current decay after channel activation in adult mdx compared with wt cardiomyocytes.

An interesting finding of the present study was the lack of an effect of extra utrophin-deficiency. Thus, the calcium channel abnormalities in only dystrophin-deficient mdx cardiomyocytes were similar as those observed in mdx-utr cardiomyocytes. We (20) and (2) have recently shown that extra utrophin-deficiency in cardiomyocytes generates significant

sodium current abnormalities in addition to those produced by dystrophin-deficiency only. This implied that utrophin exerts a regulatory effect on cardiac $Na_v1.5$ channels in dystrophin-deficient mdx mice. The data of the present study suggest that, in contrast to $Na_v1.5$, cardiac $Ca_v1.2$ calcium channels are not regulated by utrophin. Alike $Na_v1.5$, on the other hand, $Ca_v1.2$ channels are certainly regulated by dystrophin. Dystrophin-regulation of L-type calcium channels has previously been postulated also for the skeletal muscle $Ca_v1.1$ channel (18).

The mechanism underlying the abnormal calcium channel properties in dystrophic cardiomyocytes reported here remains unknown. A possible factor that may affect both current density and inactivation is calcium channel auxiliary subunit expression (26), which might be altered in dystrophic cells. Our quantitative RT-PCR experiments, however, showing that mRNAlevels of the calcium channel subunits in wt and dystrophic cardiomyocytes are similar, suggest that this is not the case. This is further supported by similar $Ca_v1.2$-α_1 (12) and $\alpha_2\delta$ auxiliary subunit (23) protein levels in normal and mdx mouse hearts. In addition, similar ON-gating charge values in wt and dystrophic cardiomyocytes, as found in the present study, suggest that altered single channel properties rather than a greater number of functional calcium channels produced the increased current density of dystrophic cells. We are currently studying alternative regulatory mechanisms which may account for the abnormal calcium channel properties in dystrophic cardiomyocytes.

Development of calcium channel abnormalities in dystrophic cardiomyocytes

In our previous study (20) we reported that L-type calcium channel abnormalities are already present in cardiomyocytes derived from neonatal dystrophic mice. Thus, in accordance with (29), we found a reduced calcium channel inactivation in neonatal dystrophic compared to wt cardiomyocytes. Since it is believed that cardiac abnormalities are not present in both the dystrophy mouse models used here even up to the young adult age (≤7 weeks) (e.g. (14; 28)), these calcium channel defects in neonatal dystrophic cardiomyocytes may be considered primary effects of the dystrophic gene mutations, which precede the development of a cardiomyopathy (20).

In the present study performed on cardiomyocytes derived from adult mice, in addition to a reduced calcium channel inactivation, we also found a considerable increase in the current density in dystrophic cardiomyocytes. In contrast, the densities of currents through calcium channels in neonatal wt and dystrophic cardiomyocytes were similar (20; 29). These findings suggest that the calcium channel abnormalities in cardiomyocytes of dystrophic mice become more severe in the adult age. A possible explanation would be that the developing pathology in the dystrophic heart generates secondary effects on the calcium channels in cardiomyocytes, i.e. perturbations in channel expression and/or function. In the failing heart, this well-known phenomenon is referred to as “electrical remodeling” (1; 17). Our data, however, do not support the hypothesis of a positive correlation between the severity of the developing cardiomyopathy and the degree of the calcium channel abnormalities observed, as would be expected for a classical remodeling effect. In particular, very similar calcium channel abnormalities were present in mdx and mdx-utr

cardiomyocytes. According to the literature, in the animal age range used for cardiomyocyte isolation in the present study (4-6 months), the mdx mouse shows only mild cardiac abnormalities (e.g. (28)), whereas in mdx-utr mice inflammation, cardiomyocyte necrosis, fibrosis and contractile dysfunction are strongly present (14; 16).

Calcium channel abnormalities in cardiomyocytes disturb the electrophysiology of the dystrophic heart

We have previously shown that reduced sodium currents in dystrophic cardiomyocytes go along with a prolonged QRS interval of the ECG in adult dystrophic mice (20). Thus, ventricular conduction is delayed in the dystrophic heart. The ECG parameters most likely to be affected by calcium channel abnormalities in dystrophic cardiomyocytes are the PQ interval and the QT interval. The former parameter reflects AV nodal conduction, whereas the latter parameter corresponds to AP duration, and is dominated by ventricular repolarization.

In the present study we show that, as an expected consequence of enhanced calcium currents in dystrophic cardiomyocytes, the PQ interval of the ECG was significantly shortened in dystrophic mice. This finding agrees with previous studies on mdx mice (e.g. (5)), and shortened PQ intervals are also observed in DMD patients (27; 33). In good accordance with the comparable calcium channel abnormalities in mdx and mdx-utr cardiomyocytes we report here, the amount of PQ interval shortening in mdx and mdx-utr compared to wt mice was also similar. Here, a limitation of our study should be noted: only cardiomyocytes isolated from the ventricles of mouse hearts, but not from the AV node were studied. Our consistent findings of shortened PQ intervals in dystrophic animals, however, suggest that similar calcium channel abnormalities (leading to enhanced calcium currents) as in ventricular cardiomyocytes are also present in myocytes of the AV node. In the present study, we also examined the development of ECG parameter abnormalities in dystrophic mice over a broad animal age range (2 to 420 days). For the PQ interval we found a significant shortening already in neonatal dystrophic mice two days after birth. This may be linked to reduced calcium channel inactivation in neonatal dystrophic cardiomyocytes (20; 29).

The QT interval of the ECG in neonatal dystrophic mice was similar to that in age-matched wt mice. In adult dystrophic mice, the QT intervals tended to be prolonged, whereby a significant difference was only reached in the oldest age group (420 days). Although not tested in the present study, this could be explained by more severe calcium channel abnormalities (stronger gain of function) in cardiomyocytes of old compared with younger dystrophic animals. As the PQ intervals, also the QT intervals of mdx and mdx-utr mice were similar. Prolonged QT intervals in adult mdx compared with wt mice have previously been reported (e.g. (5; 29)). However, the available literature is contradictory in that, for example, other authors found normal QT intervals in adult mdx mice (e.g. (12)). The lack of a significant prolongation of the QT interval in 140 day-old adult dystrophic mice reported here matches with a normal AP duration in dystrophic cardiomyocytes derived from mice of similar age, but, on the other hand, disagrees with the presence of considerable calcium channel abnormalities in these cells. This discrepancy, namely that enhanced calcium

currents in dystrophic cardiomyocytes do not induce significant AP and QT interval prolongation, may be explained by the comparably small contribution of L-type calcium currents to the short cardiac AP in the mouse (21). This possibility was tested in our AP computer simulations, which indeed showed that a 4-fold increase in g_{CaL} is needed to considerably prolong the mouse AP (Fig. 3E). On the other hand, already a 1.6-fold increase in g_{CaL} (resembling “dystrophic” calcium conductance) generated a pronounced prolongation of the simulated human cardiac AP (Fig. 3F). This is consistent with the view that, compared to the mouse, L-type calcium channel activity plays a more prominent role in shaping the long human cardiac AP (21).

Together our findings suggest that the calcium channel abnormalities we found in cardiomyocytes from 4-6 months old dystrophic mice do not suffice to significantly lengthen the AP and considerably prolong the QT interval in these animals. On the other hand, importantly, calcium channel abnormalities, if also present in dystrophic human ventricular cardiomyocytes in a comparable dimension as in the mouse, will have a dramatic effect on ventricular repolarization in the dystrophic human heart. Thus, enhanced calcium currents in dystrophic cardiomyocytes may contribute to the QT interval prolongation observed in some DMD patients (33).

Clinical implications

In the present study we have identified significant L-type calcium channel abnormalities in adult dystrophic cardiomyocytes which enhance the calcium influx during the cardiac AP. Thereby we could uncover a mechanism which may underlie part of the ECG abnormalities regularly observed in DMD mouse models and in DMD patients. Similar gain of function calcium channel abnormalities as reported herein, namely larger currents and impaired inactivation, underlie the serious cardiac arrhythmias observed in Timothy syndrome, a rare multisystem disorder caused by $Ca_v1.2$ channel mutations (3; 10; 32). Consequently, the “dystrophic” calcium channel abnormalities we report here may be considered a feasible source of cardiac arrhythmias. Finally, abnormally big L-type calcium currents in cardiomyocytes also represent a potential trigger for cardiomyopathy development (24).

Acknowledgements

We are thankful to S. Dysek (Med. Univ. Vienna), A. Lauermann (Med. Univ. Vienna), and R. Egger (Med. Univ. Innsbruck) for technical assistance.

Grants

This work was supported by the Austrian Science Fund (FWF) [P19352-B11 and P23060-B19 to K. Hilber; P24079-B21 and F4406 to G.J. Obermair; P21006-B11 to H. Todt; P19710-B02 to H. Kubista].

References

1. Aiba T, Tomaselli GF. Electrical remodeling in the failing heart. Curr Opin Cardiol. 2010; 25:29–36. [PubMed: 19907317]
2. Albesa M, Ogrodnik J, Rougier JS, Abriel H. Regulation of the cardiac sodium channel Nav1.5 by utrophin in dystrophin-deficient mice. Cardiovasc Res. 2011; 89:320–328. [PubMed: 20952415]

Europe PMC Funders Author Manuscripts

3. Barrett CF, Tsien RW. The Timothy syndrome mutation differentially affects voltage- and calcium-dependent inactivation of CaV1.2 L-type calcium channels. Proc Natl Acad Sci U S A. 2008; 105:2157–2162. [PubMed: 18250309]
4. Bondarenko VE, Szigeti GP, Bett GC, Kim SJ, Rasmusson RL. Computer model of action potential of mouse ventricular myocytes. Am J Physiol Heart Circ Physiol. 2004; 287:H1378–H1403. [PubMed: 15142845]
5. Bostick B, Yue Y, Lai Y, Long C, Li D, Duan D. Adeno-associated virus serotype-9 microdystrophin gene therapy ameliorates electrocardiographic abnormalities in mdx mice. Hum Gene Ther. 2008; 19:851–856. [PubMed: 18666839]
6. Bushby K, Finkel R, Birnkrant DJ, Case LE, Clemens PR, Cripe L, Kaul A, Kinnett K, McDonald C, Pandya S, Poysky J, et al. Diagnosis and management of Duchenne muscular dystrophy, part 2: implementation of multidisciplinary care. Lancet Neurol. 2010; 9:177–189. [PubMed: 19945914]
7. Catterall WA, Perez-Reyes E, Snutch TP, Striessnig J. International Union of Pharmacology. XLVIII. Nomenclature and structure-function relationships of voltage-gated calcium channels. Pharmacol Rev. 2005; 57:411–425. [PubMed: 16382099]
8. Cheng YJ, Lang D, Caruthers SD, Efimov IR, Chen J, Wickline SA. Focal but reversible diastolic sheet dysfunction reflects regional calcium mishandling in dystrophic mdx mouse hearts. Am J Physiol Heart Circ Physiol. 2012; 303:H559–H568. [PubMed: 22777417]
9. Deconinck AE, Rafael JA, Skinner JA, Brown SC, Potter AC, Metzinger L, Watt DJ, Dickson JG, Tinsley JM, Davies KE. Utrophin-dystrophin-deficient mice as a model for Duchenne muscular dystrophy. Cell. 1997; 90:717–727. [PubMed: 9288751]
10. Dixon RE, Cheng EP, Mercado JL, Santana LF. L-type ca(2+) channel function during timothy syndrome. Trends Cardiovasc Med. 2012; 22:72–76. [PubMed: 22999068]
11. Ervasti JM, Campbell KP. Membrane organization of the dystrophin-glycoprotein complex. Cell. 1991; 66:1121–1131. [PubMed: 1913804]
12. Gavillet B, Rougier JS, Domenighetti AA, Behar R, Boixel C, Ruchat P, Lehr HA, Pedrazzini T, Abriel H. Cardiac sodium channel Nav1.5 is regulated by a multiprotein complex composed of syntrophins and dystrophin. Circ Res. 2006; 99:407–414. [PubMed: 16857961]
13. Gee SH, Madhavan R, Levinson SR, Caldwell JH, Sealock R, Froehner SC. Interaction of muscle and brain sodium channels with multiple members of the syntrophin family of dystrophin-associated proteins. J Neurosci. 1998; 18:128–137. [PubMed: 9412493]
14. Grady RM, Teng H, Nichol MC, Cunningham JC, Wilkinson RS, Sanes JR. Skeletal and cardiac myopathies in mice lacking utrophin and dystrophin: a model for Duchenne muscular dystrophy. Cell. 1997; 90:729–738. [PubMed: 9288752]
15. Hagiwara S, Byerly L. Calcium channel. Annu Rev Neurosci. 1981; 4:69–125. [PubMed: 6261668]
16. Janssen PM, Hiranandani N, Mays TA, Rafael-Fortney JA. Utrophin deficiency worsens cardiac contractile dysfunction present in dystrophin-deficient mdx mice. Am J Physiol Heart Circ Physiol. 2005; 289:H2373–H2378. [PubMed: 16024571]
17. Jeyaraj D, Wan X, Ficker E, Stelzer JE, Deschenes I, Liu H, Wilson LD, Decker KF, Said TH, Jain MK, Rudy Y, et al. Ionic bases for electrical remodeling of the canine cardiac ventricle. Am J Physiol Heart Circ Physiol. 2013; 305:H410–H419. [PubMed: 23709598]
18. Johnson BD, Scheuer T, Catterall WA. Convergent regulation of skeletal muscle Ca2+ channels by dystrophin, the actin cytoskeleton, and cAMP-dependent protein kinase. Proc Natl Acad Sci U S A. 2005; 102:4191–4196. [PubMed: 15753322]
19. Kato Y, Masumiya H, Agata N, Tanaka H, Shigenobu K. Developmental changes in action potential and membrane currents in fetal, neonatal and adult guinea-pig ventricular myocytes. J Mol Cell Cardiol. 1996; 28:1515–1522. [PubMed: 8841938]
20. Koenig X, Dysek S, Kimbacher S, Mike AK, Cervenka R, Lukacs P, Nagl K, Dang XB, Todt H, Bittner RE, Hilber K. Voltage-gated ion channel dysfunction precedes cardiomyopathy development in the dystrophic heart. PLoS ONE. 2011; 6:e20300. [PubMed: 21677768]
21. Koivumaki JT, Takalo J, Korhonen T, Tavi P, Weckstrom M. Modelling sarcoplasmic reticulum calcium ATPase and its regulation in cardiac myocytes. Philos Transact A Math Phys Eng Sci. 2009; 367:2181–2202.

22. Lloyd CM, Lawson JR, Hunter PJ, Nielsen PF. The CellML Model Repository. Bioinformatics. 2008; 24:2122–2123. [PubMed: 18658182]
23. Lohan J, Culligan K, Ohlendieck K. Deficiency in Cardiac Dystrophin Affects the Abundance of the α-/β-Dystroglycan Complex. J Biomed Biotechnol. 2005; 2005:28–36. [PubMed: 15689636]
24. Muth JN, Bodi I, Lewis W, Varadi G, Schwartz A. A Ca(2+)-dependent transgenic model of cardiac hypertrophy: A role for protein kinase Calpha. Circulation. 2001; 103:140–147. [PubMed: 11136699]
25. Nerbonne JM, Nichols CG, Schwarz TL, Escande D. Genetic manipulation of cardiac K(+) channel function in mice: what have we learned, and where do we go from here? Circ Res. 2001; 89:944–956. [PubMed: 11717150]
26. Obermair GJ, Tuluc P, Flucher BE. Auxiliary Ca(2+) channel subunits: lessons learned from muscle. Curr Opin Pharmacol. 2008; 8:311–318. [PubMed: 18329337]
27. Perloff JK. Cardiac rhythm and conduction in Duchenne's muscular dystrophy: a prospective study of 20 patients. J Am Coll Cardiol. 1984; 3:1263–1268. [PubMed: 6707378]
28. Quinlan JG, Hahn HS, Wong BL, Lorenz JN, Wenisch AS, Levin LS. Evolution of the mdx mouse cardiomyopathy: physiological and morphological findings. Neuromuscul Disord. 2004; 14:491–496. [PubMed: 15336690]
29. Sadeghi A, Doyle AD, Johnson BD. Regulation of the cardiac L-type Ca2+ channel by the actin-binding proteins alpha-actinin and dystrophin. Am J Physiol Cell Physiol. 2002; 282:C1502–C1511. [PubMed: 11997265]
30. Schlick B, Flucher BE, Obermair GJ. Voltage-activated calcium channel expression profiles in mouse brain and cultured hippocampal neurons. Neuroscience. 2010; 167:786–798. [PubMed: 20188150]
31. Sicinski P, Geng Y, Ryder-Cook AS, Barnard EA, Darlison MG, Barnard PJ. The molecular basis of muscular dystrophy in the mdx mouse: a point mutation. Science. 1989; 244:1578–1580. [PubMed: 2662404]
32. Splawski I, Timothy KW, Sharpe LM, Decher N, Kumar P, Bloise R, Napolitano C, Schwartz PJ, Joseph RM, Condouris K, Tager-Flusberg H, et al. Ca(V)1.2 calcium channel dysfunction causes a multisystem disorder including arrhythmia and autism. Cell. 2004; 119:19–31. [PubMed: 15454078]
33. Spurney CF. Cardiomyopathy of Duchenne muscular dystrophy: current understanding and future directions. Muscle Nerve. 2011; 44:8–19. [PubMed: 21674516]
34. ten Tusscher KH, Noble D, Noble PJ, Panfilov AV. A model for human ventricular tissue. Am J Physiol Heart Circ Physiol. 2004; 286:H1573–H1589. [PubMed: 14656705]
35. Venetucci L, Denegri M, Napolitano C, Priori SG. Inherited calcium channelopathies in the pathophysiology of arrhythmias. Nat Rev Cardiol. 2012; 9:561–575. [PubMed: 22733215]
36. Viola HM, Davies SM, Filipovska A, Hool LC. L-type Ca2+ channel contributes to alterations in mitochondrial calcium handling in the mdx ventricular myocyte. Am J Physiol Heart Circ Physiol. 2013; 304:H767–H775. [PubMed: 23335798]
37. Wei X, Neely A, Lacerda AE, Olcese R, Stefani E, Perez-Reyes E, Birnbaumer L. Modification of Ca2+ channel activity by deletions at the carboxyl terminus of the cardiac alpha 1 subunit. J Biol Chem. 1994; 269:1635–1640. [PubMed: 7507480]
38. Williams IA, Allen DG. Intracellular calcium handling in ventricular myocytes from mdx mice. Am J Physiol Heart Circ Physiol. 2007; 292:H846–H855. [PubMed: 17012353]
39. Woolf PJ, Lu S, Cornford-Nairn R, Watson M, Xiao XH, Holroyd SM, Brown L, Hoey AJ. Alterations in dihydropyridine receptors in dystrophin-deficient cardiac muscle. Am J Physiol Heart Circ Physiol. 2006; 290:H2439–H2445. [PubMed: 16415078]

Europe PMC Funders Author Manuscripts

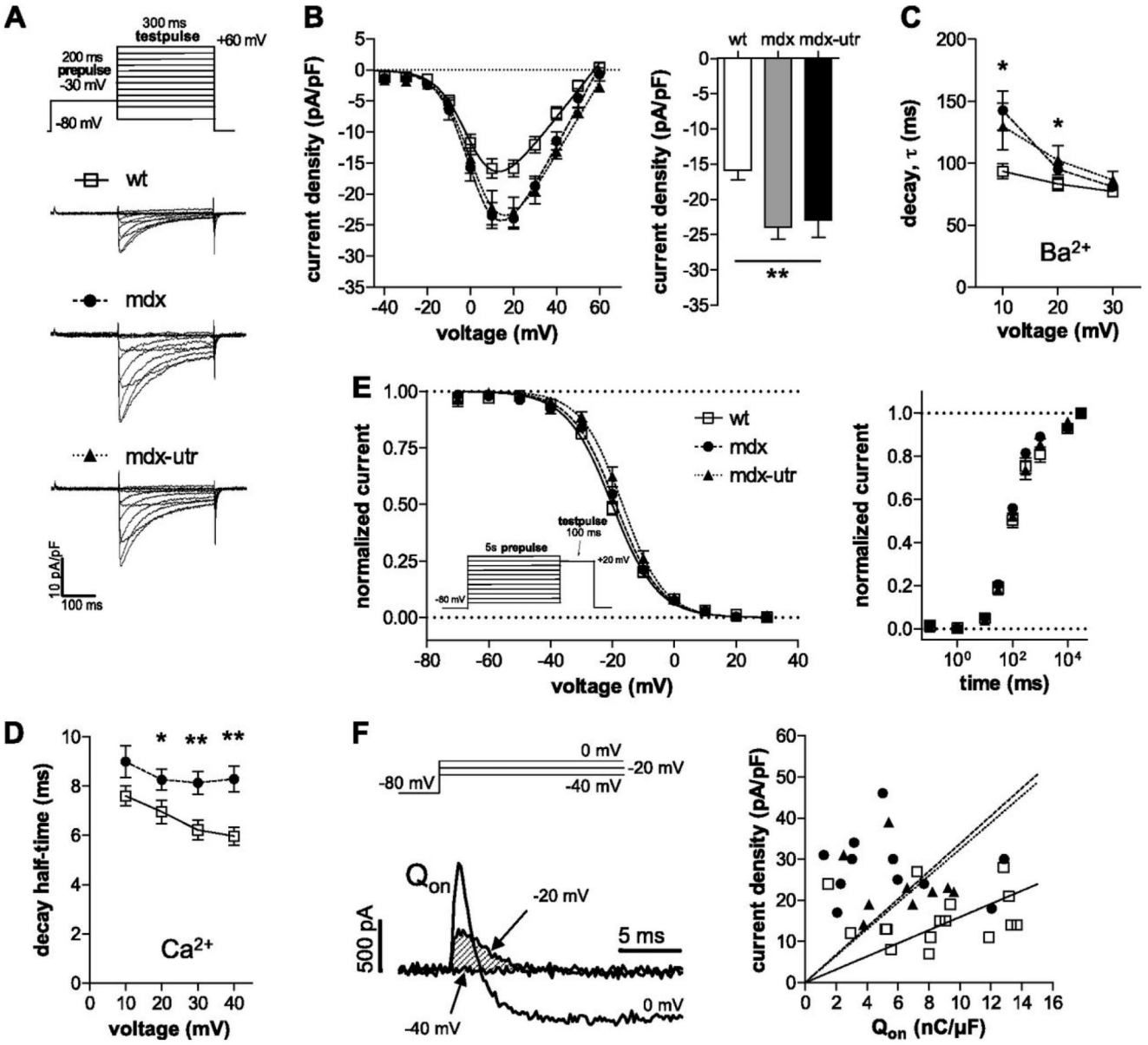

Figure 1.

L-type calcium channel properties in wt and dystrophic cardiomyocytes. A: Original traces of barium currents of a typical wt, mdx, and mdx-utr cardiomyocyte elicited by the pulse protocol displayed on top. A prepulse prior to the test pulses was applied to exclude a possible contamination by T-type calcium currents. B: Current density-voltage relationships of wt and dystrophic cardiomyocytes (left). On the right, a comparison of the current densities at +20 mV is shown. ANOVA revealed a significant difference (** $p<0.01$) between the three tested groups. Tukey's Post Hoc test yielded significant differences both between mdx and wt ($p<0.01$), and between mdx-utr and wt ($p<0.05$), but not between mdx and mdx-utr. Fits of the current-voltage relationships (see Methods) revealed the following parameters for wt (n=16), mdx (n=11), and mdx-utr (n=9) cardiomyocytes, respectively:

$V_{0.5}$ (mV): 2 ± 1, 3 ± 2, 4 ± 1 (n.s.); K (mV): 7.0 ± 0.3, 6.6 ± 0.4, 7.1 ± 0.4 (n.s.); V_{rev} (mV): 57 ± 2, 59 ± 2, 63 ± 1 ($p<0.05$, ANOVA). Cell capacitance values were similar and amounted to 68 ± 4 pF in wt, 73 ± 8 pF in mdx, and 70 ± 5 pF in mdx-utr cardiomyocytes. C: Comparison of the barium current decay kinetics between wt and dystrophic cardiomyocytes at various membrane voltages (*$p<0.05$, ANOVA). **τ**-values were derived from single exponential fits of the current decay after channel activation. D: Comparison of the calcium current decay kinetics between wt (n=20) and dystrophic mdx (n=24) cardiomyocytes at various voltages (*$p<0.05$, **$p<0.01$; t-test). Decay half-time represents the time period between the current peak and the time point at which the current had decayed to 50%. The calcium current densities at +30 mV (voltage at which current was maximal) amounted to -6.6 ± 0.5 pA/pF in wt and -9.3 ± 1.1 pA/pF in mdx cardiomyocytes and were significantly different ($p<0.05$). E: Voltage-dependence of barium current steady-state inactivation for wt and dystrophic cardiomyocytes (left). Data fits with a Boltzmann function (see Methods) revealed the following parameters for wt (n=6), mdx (n=7), and mdx-utr (n=8) cardiomyocytes, respectively: $V_{0.5}$ (mV): -20 ± 1, -19 ± 1, -17 ± 1 (n.s.); K (mV): 7.4 ± 0.3, 7.7 ± 0.7, 6.5 ± 0.3 (n.s.). The recovery from inactivation in wt (n=8) and dystrophic (mdx, n=8; mdx-utr, n=11) cardiomyocytes is shown on the right. Here the peak currents elicited by the test pulse were normalized to the maximum peak current and plotted against recovery time. F: Original current traces (left) elicited by depolarizing voltage steps to -40, -20, and 0 mV from a holding potential of -80 mV. Such experiments were performed in all cells from which also current density-voltage relationships were derived (see Fig. 1B). An outward gating current without “contamination” by barium inward current can be observed at a potential of -20 mV. On-gating charge (Q_{on}) was determined as the time integral of the outward gating current at -20 mV (shaded area in the left figure part), and normalized to the cell capacitance. The Q_{on} values amounted to 8.5 ± 0.9 nC/µF (n=16) in wt, 5.6 ± 1.2 nC/µF (11) in mdx, and 6.3 ± 0.8 nC/µF (9) in mdx-utr (p=0.1, ANOVA). Individual Q_{on} values of all experiments were plotted against the respective current densities at +20 mV.

Europe PMC Funders Author Manuscripts

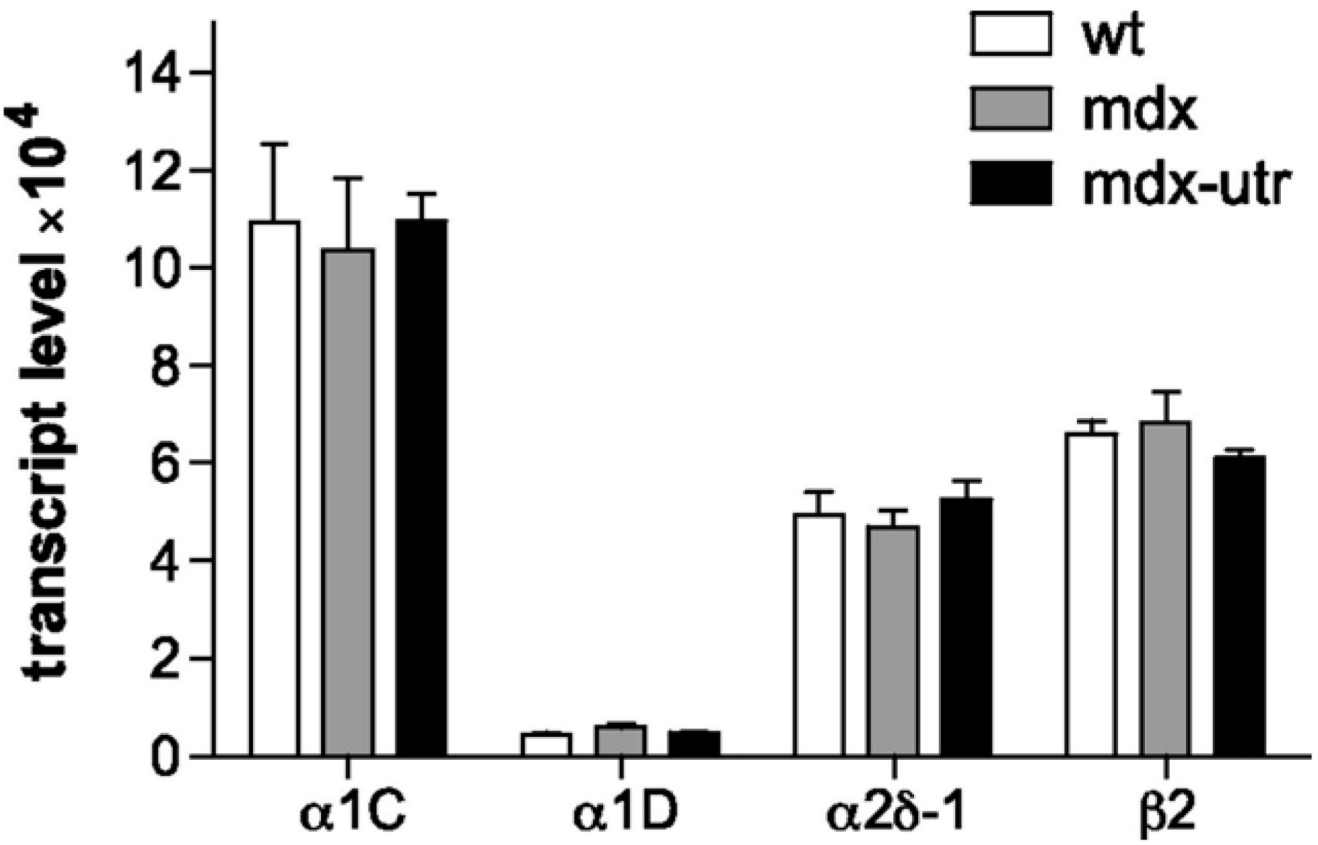

Figure 2.

L-type calcium channel subunit mRNA levels in wt, mdx, and mdx-utr adult cardiac ventricles. Three hearts per genotype were used for TaqMan quantitative RT-PCR for the main ventricular α_1-subunit $Ca_v1.2$ (α_{1C}), the α_1-subunit $Ca_v1.3$ (α_{1D}), and the auxiliary subunits $\alpha_2\delta$-1 and β_2. The relative transcript levels were normalized to the two most stably expressed endogenous control genes Hprt1 and Gapdh, and bars represent means ± SEM. mRNA for $Ca_v1.2$ was the most abundant α_1 subunit transcript, while $Ca_v1.3$ mRNA accounted for only ~5% of L-type calcium channel transcripts. There was neither a difference in the overall ($p=0.82$) nor in the specific (α_1, $\alpha_2\delta$-1, and β_2; $p=0.87$) subunit transcript levels between wt, mdx, and mdx-utr hearts (two-way ANOVA).

Europe PMC Funders Author Manuscripts

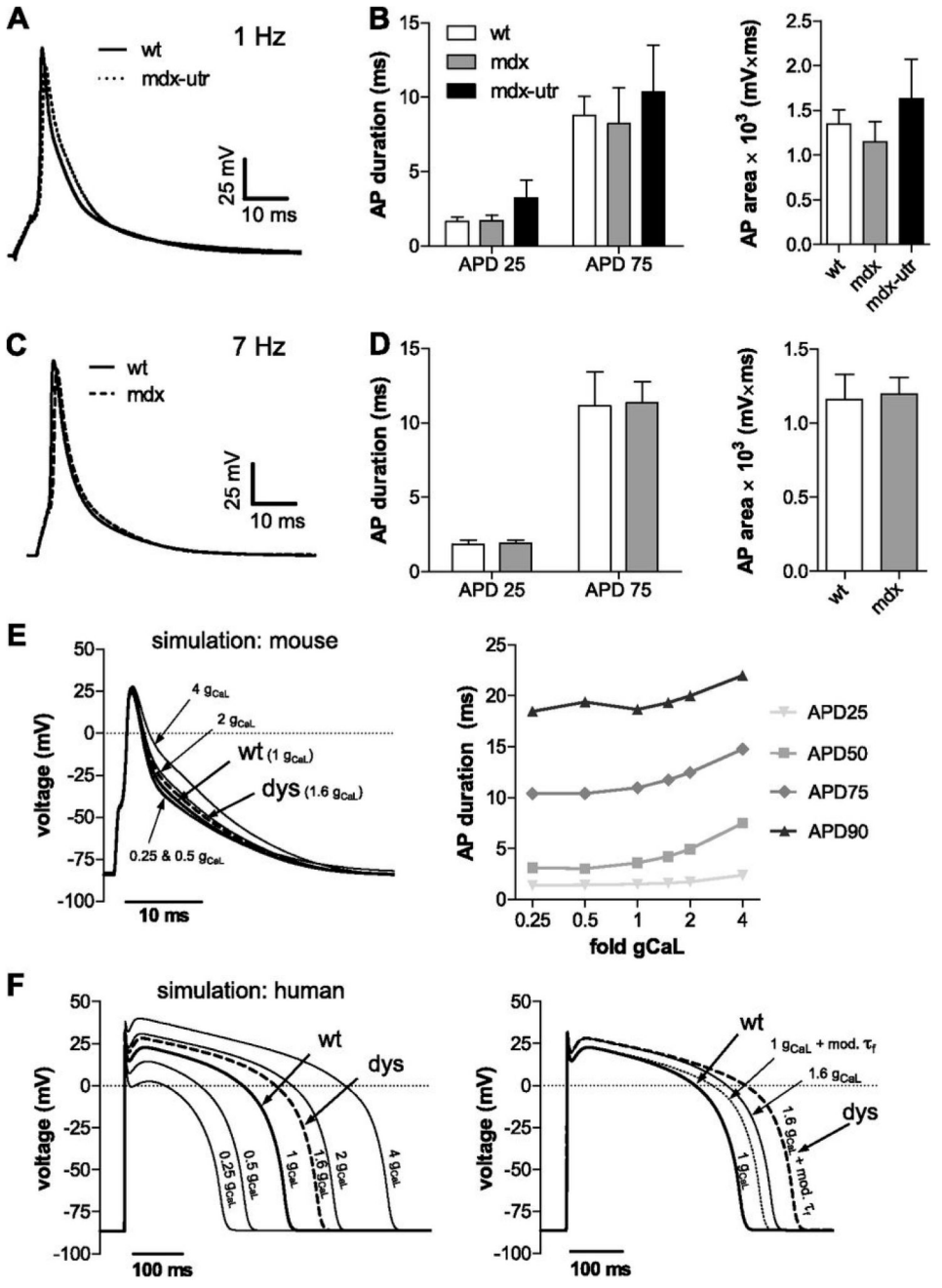

Figure 3.

Action potentials (APs) in wt and dystrophic cardiomyocytes. A: Typical APs recorded from a wt and a mdx-utr cardiomyocyte which were elicited by a 4 ms current injection at 125 % threshold at 1 Hz pacing frequency. B: AP duration (left) was evaluated from the maximum depolarization value reached to the time point at which 25 % (APD25) and 75 % (APD75) of repolarization had been accomplished. AP area (mV*ms) (right) was determined by integrating from the start of the current stimulus to the very end of repolarization. ANOVA did not reveal significant differences between wt (n=8) and dystrophic (mdx, n=7; mdx-utr,

n=8) cardiomyocytes. C: APs recorded from a wt and a mdx cardiomyocyte at 7 Hz pacing frequency. D: Corresponding AP analyses performed as in B. No significant differences existed between wt (n=12) and dystrophic (mdx, n=13) cardiomyocytes. E: AP simulation using a computer model of a mouse ventricular cardiomyocyte (4). The experimentally determined 1.6-fold increase in current density of dystrophic (dys) cardiomyocytes (similar in mdx and mdx-utr, Fig. 1B) was implemented into the model by changing the respective default conductance, g_{CaL}=0.173 mS/μF to g_{CaL}=0.277 mS/μF. In addition, g_{CaL} values were systematically varied between 0.25- and 4-fold of the default value. Their impact on AP durations for different repolarization levels (25 – 90%) is displayed on the right. F: AP simulation (left) performed as in E using a computer model of a human ventricular cardiomyocyte (34). On the right, in addition to the increased "dystrophic" current density (1.6 g_{CaL}, solid line), the decelerated "dystrophic" current decay (Fig. 1C) (1 g_{CaL} + mod. τ_f, dotted line) was implemented into the model (see Materials and methods). The dashed line (dys) represents the implementation of both "dystrophic" effects together.

Europe PMC Funders Author Manuscripts

Europe PMC Funders Author Manuscripts

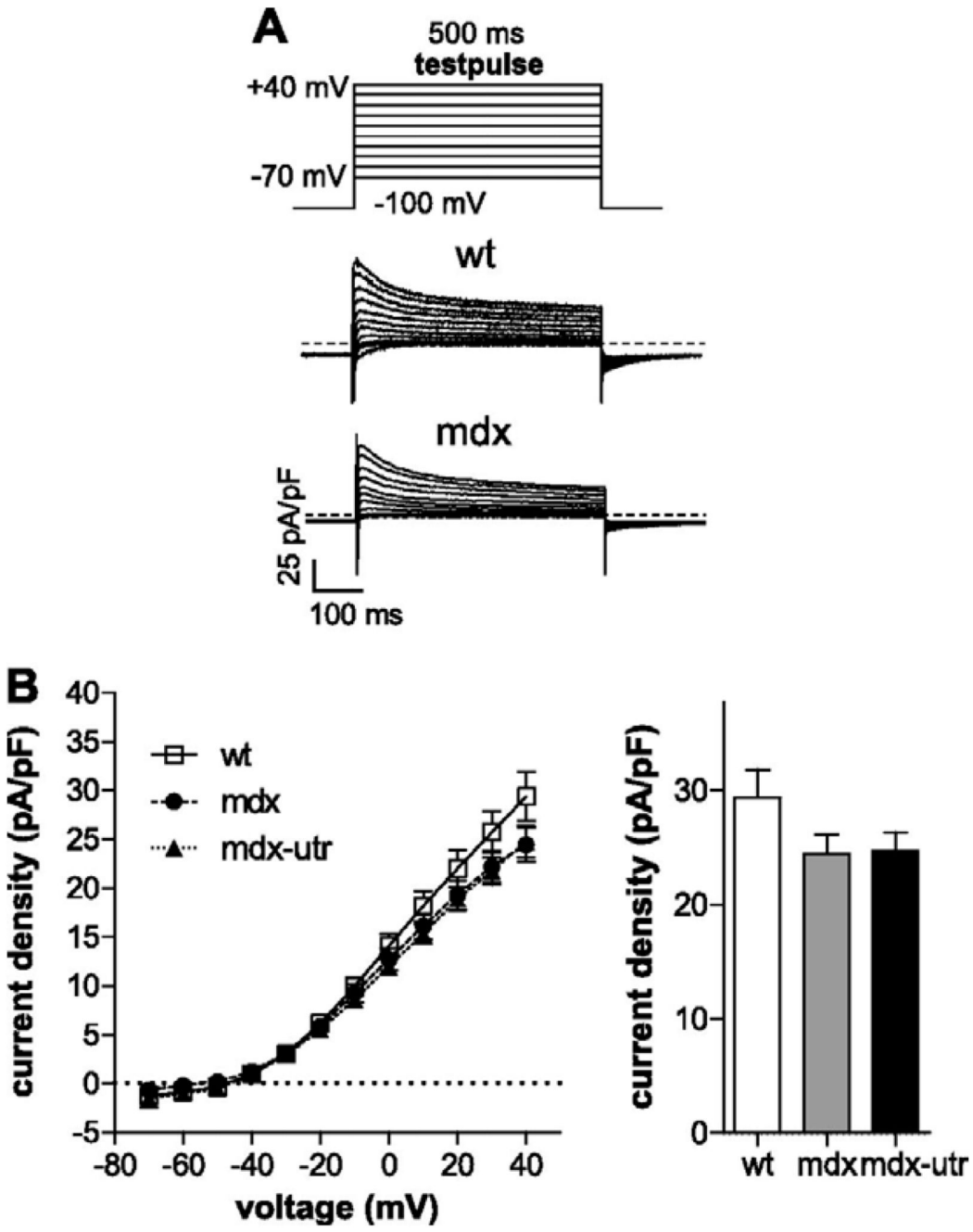

Figure 4.

Potassium currents in wt and dystrophic cardiomyocytes. A: Typical original potassium current traces of a wt and a mdx cardiomyocyte elicited from a holding potential of -100 mV by various depolarizing voltage steps of 500 ms duration. The dashed lines indicate the zero current level. B (left): Current density–voltage relationships derived from a series of experiments (n=14 for wt, 16 for mdx, and 14 for mdx-utr) as shown in A. The current levels were determined at the end of the test pulse. On the right, the current density values at +40

mV are compared between wt and dystrophic cardiomyocytes. ANOVA did not reveal a significant difference between the tested groups (p=0.16).

Europe PMC Funders Author Manuscripts

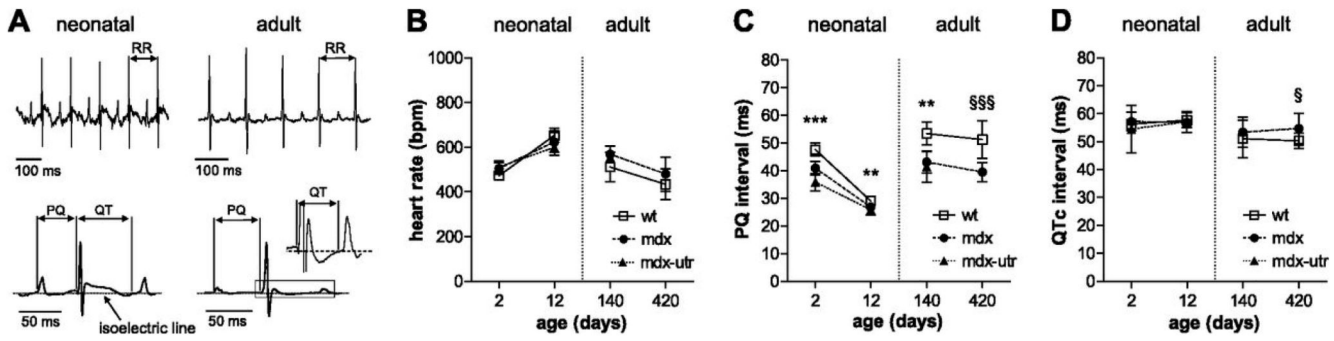

Figure 5.

Surface ECG parameters of neonatal and adult wt and dystrophic mice. A: Typical original ECG signals from first standard lead (aI) for a neonatal (left) and an adult (right) wt mouse, and the corresponding averaged signals of 100 beats (lower panel), respectively. B: Heart rate in bpm is plotted over a broad animal age range for wt, mdx, and mdx-utr neonatal and adult animals. The number of animals per age and per genotype was 4-10 and 4-23 for neonatal and adult, respectively. ANOVA revealed no significant differences between the three groups ($p>0.05$). C: PQ intervals are plotted over animal age for wt, mdx and mdx-utr mice. ** and *** indicate that ANOVA revealed a significant difference ($p<0.01$ and $p<0.001$, respectively). Tukey's Post Hoc test was always significant between mdx and wt, and between mdx-utr and wt, but not between mdx and mdx-utr. §§§ indicates that a t-test revealed a significant difference ($p<0.001$). D: Heart rate corrected QT intervals (QTc) are plotted over animal age for wt, mdx, and mdx-utr mice. § indicates that a t-test revealed a significant difference ($p<0.05$). Mean values ± STD of all animals of a given genotype are displayed.